Laser and Particle Beams (2001), *19*, 309–316. Printed in the USA.

Low microdivergence medium-mass ion beam produced from a N_2O cryogenic diode

KOICHI KASUYA, YOHSUKE KISHI, TAKAHIRO KAMIYA, AND MASATO FUNATSU

Department of Energy Sciences, Tokyo Institute of Technology, Nagatsuta 4259, Midori-ku, Yokohama, Kanagawa, Japan 226-8502

(RECEIVED 26 May 2000; ACCEPTED 16 February 2001)

Abstract

Medium-mass ion beams including nitrogen and oxygen were produced from a cryogenic diode with N_2O ice as the ion source. The nominal diode voltage was 300–400 kV, and the peak ion current was 240 A. The beam divergence angle was measured with a five-aperture time-integrated pinhole camera. The five camera images were analyzed to estimate the spatial distribution of the beam source divergence angle along the anode radius, yielding a value of 5–6 mrad for the average microdivergence. This is low enough for this ion source to be studied further in the near future. If possible, we want to consider this as one of the probable candidate ion sources for ion beam drivers for future inertial confinement fusion (ICF) and inertial fusion energy (IFE) applications.

Keywords: Microdivergent angle; Nitrogen ion beam; Cryogenic diode; Arrayed pinhole camera; Solid-state track detector

1. INTRODUCTION AND MOTIVATION

The top laboratories for the pulsed ion beam research works were Sandia National Laboratories at Albuquerque, NM, USA (Quintenz *et al.*, 1996). Light ion beams were also investigated in many laboratories as were shown by Bluhm (1992) and Greenly *et al.* (1988), for example. Most recent topics concerning such ion beams were reviewed by Olson (1999) and Cuneo *et al.* (1999*a*,*b*).

Although the following claims regarding light and heavy ion beams may not be totally accurate, they want to mention that their motivation to start the research work described in this article is as follows. Also, as this paper is neither a review paper nor a discussion paper which deals mainly with the comparison of both kinds of ion beams, the authors want to lay stress on their motivation.

Although beam production costs for light ion-driven inertial confinement fusion (ICF) and inertial fusion energy (IFE) are less than for heavy ion fusion (HIF), the higher charge-to-mass ratio may restrict the ultimate focusability of such a beam on ICF and IFE targets under a simple and qualitative consideration. On the other hand, the high beam production cost of an HIF driver, together with questions about whether the currents required are achievable, lead to concerns about whether heavy ion beams are the most promising candidate for a future particle beam driver. Of course, this comes under a simple and qualitative consideration and this is not the main concern of this paper. Because of these considerations, a medium-mass ion beam may have the best focusability and the cost compromise in the future. Thus, we discuss here the production of such a medium-mass pulsed ion beam from a cryogenic ion source, and measurement of the beam divergence angle both at the source and at a short propagation distance. This work is a continuation of earlier experiments by Kasuya and Mitobe (1987) and Hanson *et al.* (1991), where pure nitrogen beams were produced from cryogenically cooled anodes.

2. EXPERIMENTAL APPARATUS

Figure 1 shows a schematic diagram of our pulsed ion beam generator. The nominal specification of the Marx generator was 1 MV, 3.75 kJ, and 0.2 Hz (repetition frequency). The line impedance of the pulse forming line (PFL) and transmission line (TL) was 5Ω, while the pulse width of them was 60 ns. A water gap switch was placed between the PFL and TL, and a magnetically insulated diode of beam extraction type was installed in the vacuum chamber. The anode was fed by this pulsed power apparatus and the ion beam was extracted in a ring shape. The electron current in the

Address correspondence and reprint requests to: Koichi Kasuya, Department of Energy Sciences, Tokyo Institute of Technology, Nagatsuta 4259, Midori-ku, Yokohama, Kanagawa, Japan 226-8502. E-mail: kkasuya@es.titech.ac.jp

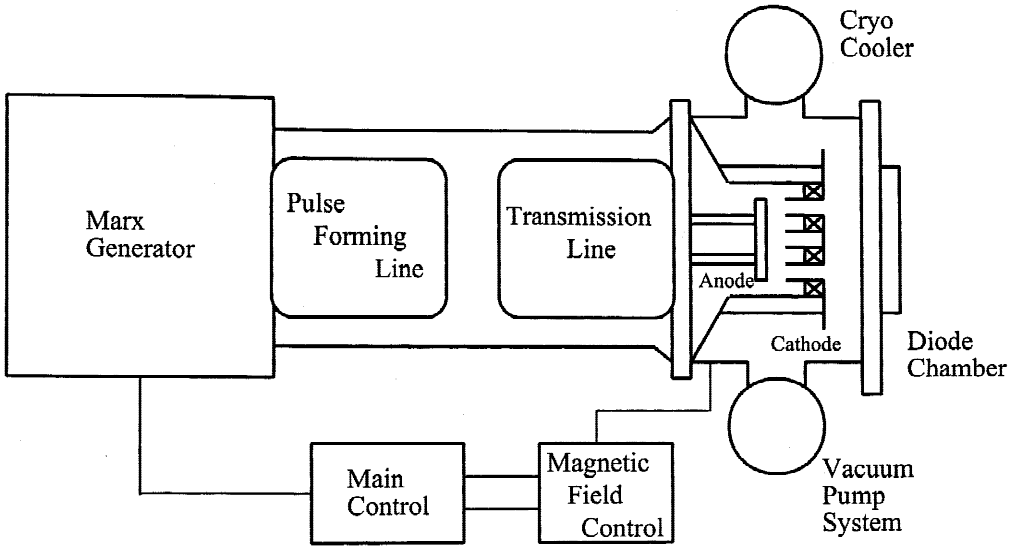

Fig. 1. Schematic diagram of the pulsed ion beam generator.

diode was suppressed by a pair of magnetic coils fed by an external capacitor bank. Both the Marx generator and the bank were triggered with a proper time delay. The vacuum chamber was evacuated by a turbo-molecular pump.

A cross-sectional view of the diode section is shown in Figure 2. The inner and outer diameters of the ring-shaped anode ion source were 122 and 98 mm, respectively. The anode was cooled by a refrigerator system which circulated helium gas between the cold head and the anode. A secondary thermal shroud with liquid nitrogen cooling was used to suppress the heat flux to the anode.

Figure 3 shows the vapor pressure of various materials as a function of temperature. Curves for four kinds of materials (H_2, N_2, N_2O, and H_2O) are compared in the same figure. The X–Y plot of the material characteristic temperature is shown in Figure 4, where X and Y correspond to the temperature for the equilibrium vapor pressure of 1×10^{-4} Torr and the material melting point. Both temperatures of liquid

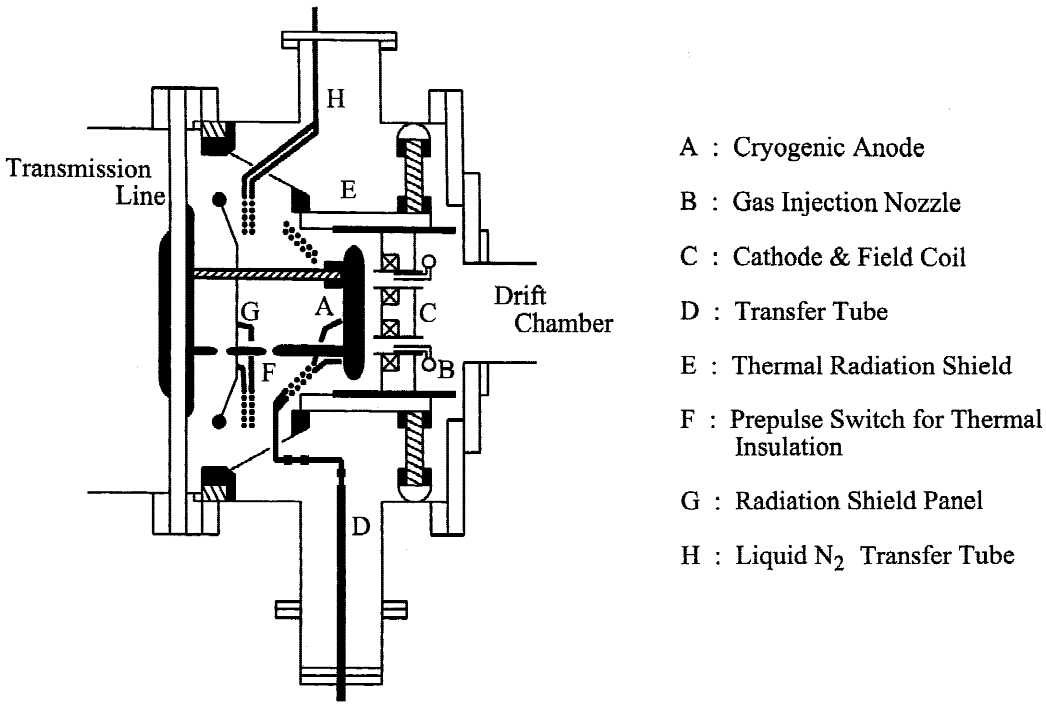

Fig. 2. Cross-sectional view of the cryogenic diode.

https://doi.org/10.1017/S0263034601192207 Published online by Cambridge University Press

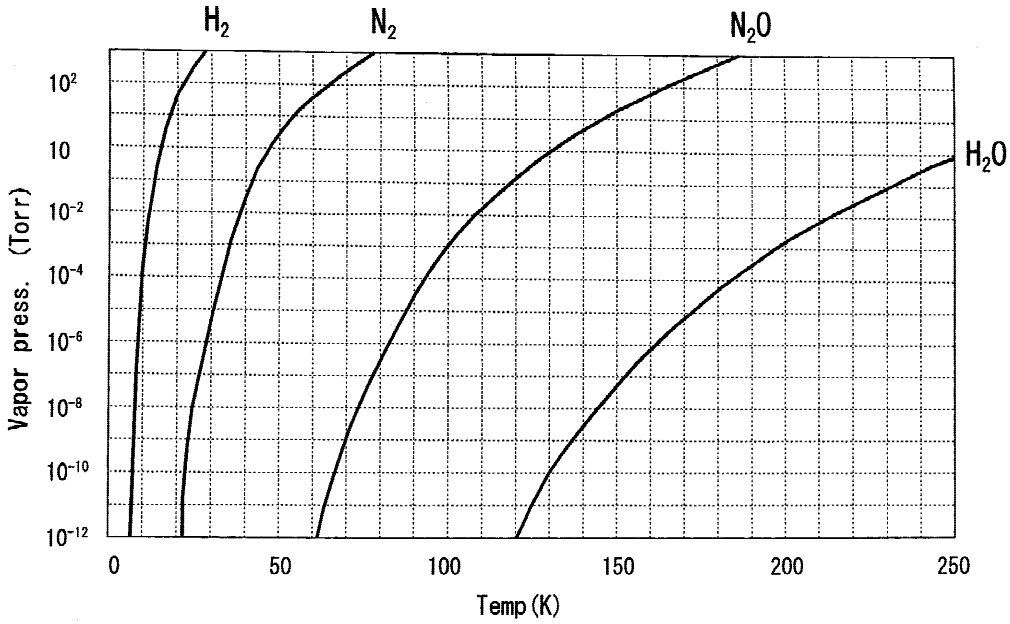

Fig. 3. Equilibrium vapor pressure.

He and liquid N_2 are also shown here. H_2O, CO_2, and N_2O can be used on the anode surface under liquid N_2 cooling, while Xe, Kr, Ar, N_2, O_2, and H_2 can be used on the anode surface under the liquid He cooling.

The schematic diagram of a Thomson parabola ion spectrometer (TPIS) is shown in Figure 5 (Kasuya *et al.*, 1999). The structure of the spectrometer is shown in detail in the same figure. Conventional solid state track detectors (CR-39 plastic plates) were used to record the time-integrated parabolas. We have a plan to use CCD elements in place of CR-39 plate in the near future. In this case, various signal noises must be kept low to obtain reasonable ion beam signals.

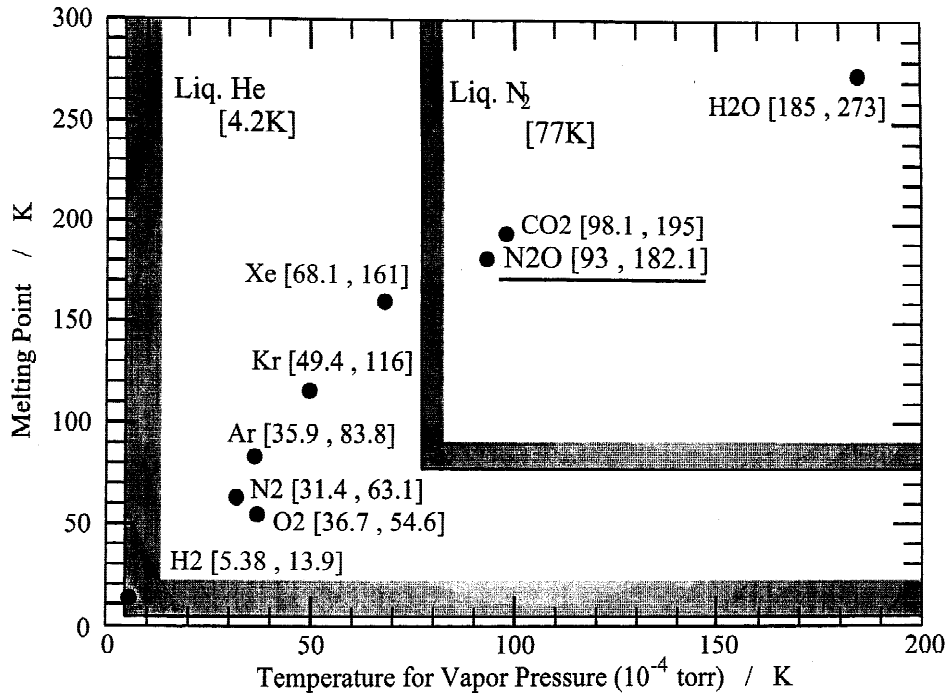

Fig. 4. Useful materials for ion sources and characteristic temperature.

https://doi.org/10.1017/S0263034601192207 Published online by Cambridge University Press

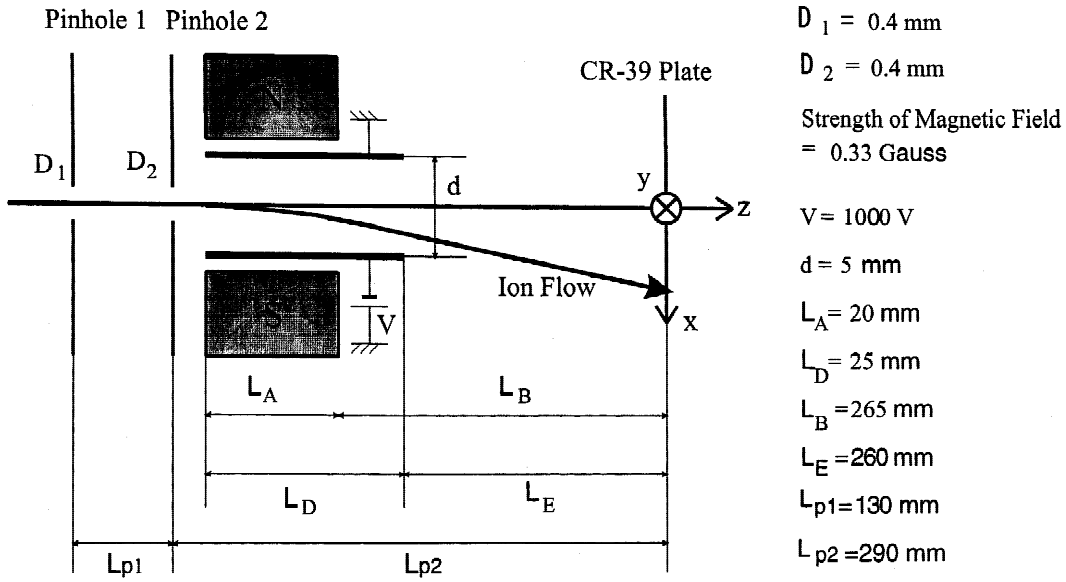

Fig. 5. Schematic diagram of Thomson parabola ion spectrometer (TPIS).

We adopted two kinds of geometry for the beam divergence diagnostics, as are shown in Figures 6 and 7. CR-39 plates were used to record the time-integrated ion tracks in both diagnostics. Figure 6 depicts the arrangement for the arrayed pinhole camera together with the anode of the diode, and Figure 7 shows the arrangement for the single pinhole camera which is mounted at the end of the beam collimator. A pair of coaxial cathodes (which were made with stainless steel pipes with different diameters, and which were placed between the inner and outer magnetic field coils) are not shown in Figures 6 and 7. A birds-eye view of the arrayed pinhole camera is also shown in Figure 6.

3. EXPERIMENTAL RESULTS OF MEDIUM-MASS ION BEAM GENERATION

The vacuum pressure of the diode chamber was 5.1×10^{-5} Torr, and was maintained with turbo-molecular pumps. The lowest anode temperature obtained was 53.7 K. This is too high a temperature for the stable formation of, say, ni-

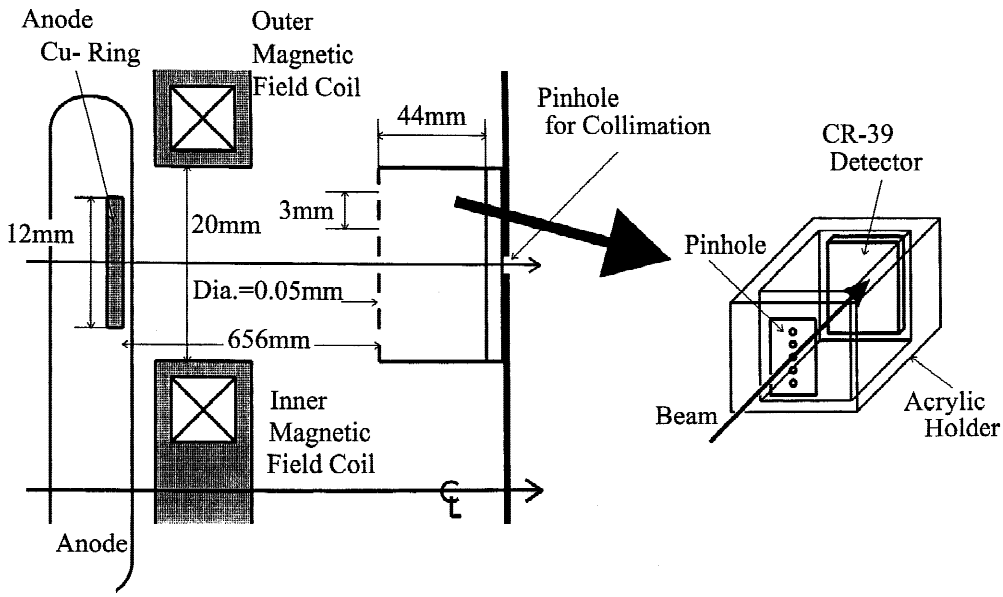

Fig. 6. Cross-sectional and bird's-eye views of arrayed pinhole camera.

https://doi.org/10.1017/S0263034601192207 Published online by Cambridge University Press

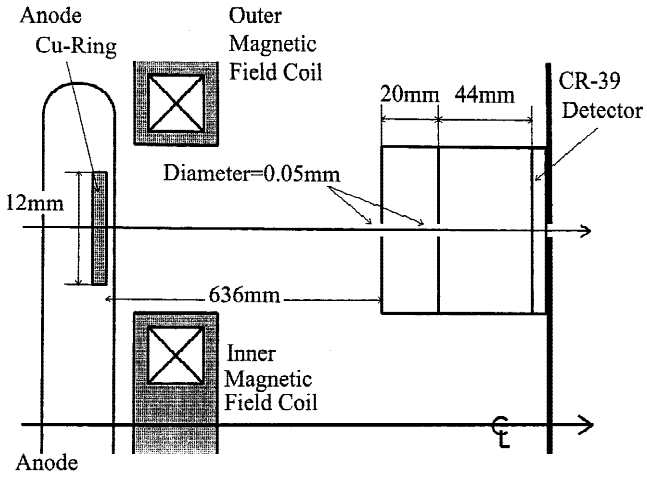

Fig. 7. Second pinhole camera and pulsed ion diode.

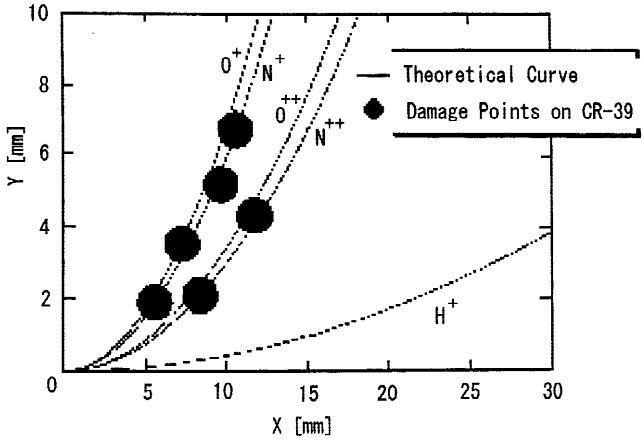

Fig. 9. Examples of ion tracks on TPIS.

trogen ice. However, as shown in Figure 3, the equivalent temperature of the N_2O ice is 88 K for the equilibrium vapor pressure of 5.1×10^{-5}, so the anode temperature was low enough to get stable formation of solid N_2O. We therefore used N_2O as our ion source material. The color of the ice formed was white.

Typical CRT traces of the transmission line voltage and the ion current are shown in Figure 8. We placed a beam ion collector (BIC) 60 cm from the anode. The offset in time between the diode voltage and ion beam current came from the time of flight of the ion beam to the BIC. The output voltage of the Marx generator was about 600 kV, the peak voltage of the transmission line was 353 kV, and the peak ion current (the second peak at 360 ns) was about 240 A. The second peak was also double humped, which included the singly and doubly ionized medium-mass ion beam. Most of the beam was composed of nitrogen, while a small part (maybe one-third) was oxygen. The first peak corresponded to the proton beam in this figure, where the proton was introduced to get a timing marker. We did not have this kind of impurity peak if we extracted ion beams from the pure anode without water ice inclusion.

Figure 9 shows examples of the ion tracks on the detector plate of the TPIS. Separation between the singly and doubly ionized beams was obtained while the separation between the N and O groups was ambiguous. The diameter of the black dots corresponds to the spatial resolution of this diagnostic system.

An example of the pinhole camera images under the arrangement of Figure 6 is shown in Figure 10, which was analyzed as a 1.5×1.5 mm area on the anode. In this case, the pinholes with 50-μm diameter and 3-mm separation distance were placed on an aluminum thin foil. The plastic for beam detection was CR-39 or of the similar material. After the analysis of Figure 10 with a particle counter, we obtained image intensity profiles as a function of location on the particle detector (Fig. 11). We analyzed Figure 11 under the assumption that the ion intensity profile is similar to a Gaussian profile. We obtained the beam intensity profile as a function of radial position on the anode surface, as is shown in Figure 12. With this series of profiles, we then obtained the beam divergence angle along the radial direc-

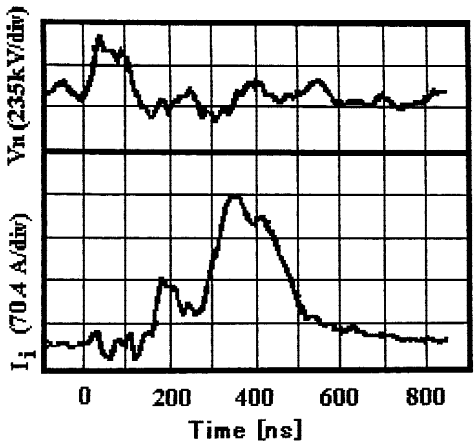

Fig. 8. Typical CRT traces of transmission-line voltage and ion current.

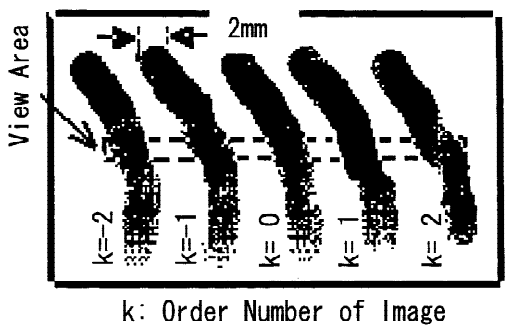

Fig. 10. Examples of ion tracks on arrayed pinhole camera.

https://doi.org/10.1017/S0263034601192207 Published online by Cambridge University Press

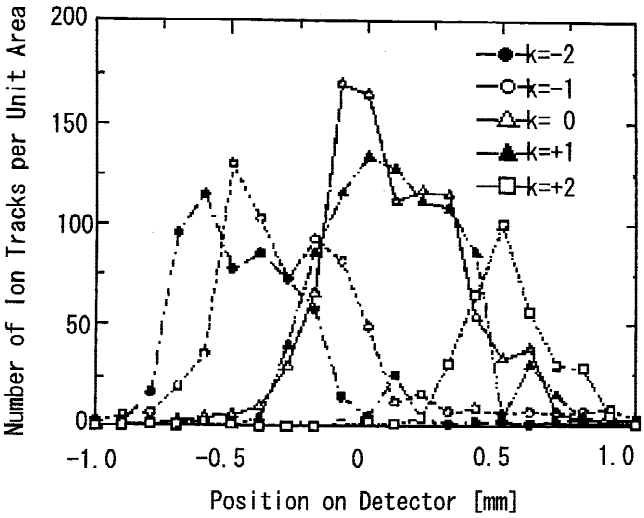

Fig. 11. Beam intensity profile behind respective pinhole.

tion of the anode surface. An example of the results is shown in Figure 13. The source divergence angle was 3–6 mrad in this figure. As was described by Mehlhorn (1997), this is an acceptable value for consideration of this source as ICF and IFE drivers.

A pinhole camera image was taken also under the arrangement of Figure 7, from which we obtained the beam intensity profile, shown in Figure 14, and measured the divergence angle after a short propagation distance. The value of the angle was estimated to be 2.55 mrad.

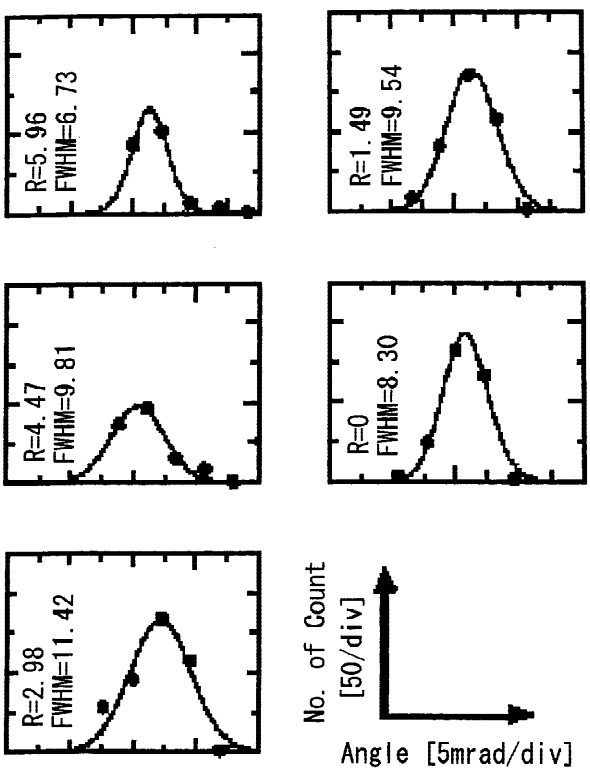

Fig. 12. Beam profile at respective radial position.

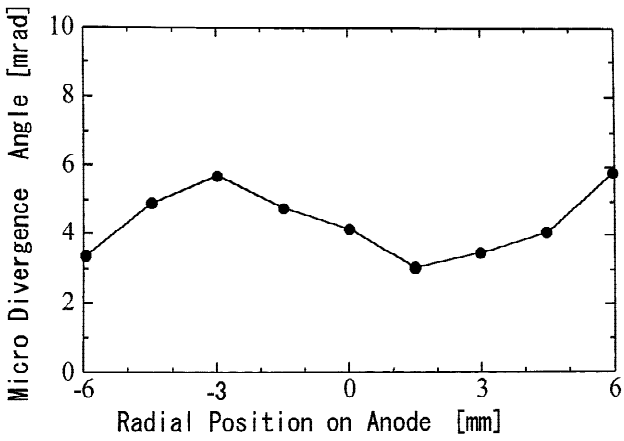

Fig. 13. Microdivergence angle versus anode radial position.

4. COMPARISON WITH PROTON BEAM DIVERGENCE

The same kinds of experiments were performed to measure the microdivergence angle of a proton beam. The ion source on the anode surface in this case was wax. Measurements with the Thomson Parabola determined the beam composition to be proton and carbon. The main part of measured beam was proton with 100–200 keV energy and 16.9 A/cm^2 ion current density. The five-aperture arrayed pinhole camera was placed 225 mm from the anode surface. At this short distance, one shot was sufficient to obtain enough data. After Gaussian shape fitting of the beam flux distributions as shown above, we obtained the beam intensity profile as a

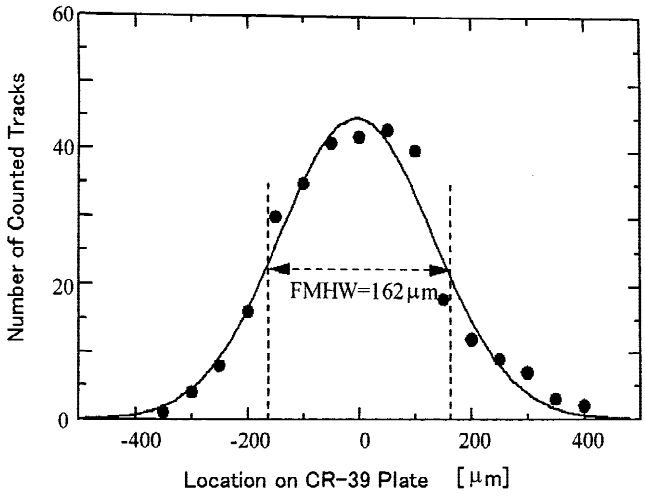

Fig. 14. Beam intensity profile on CR-39 detector plate.

https://doi.org/10.1017/S0263034601192207 Published online by Cambridge University Press

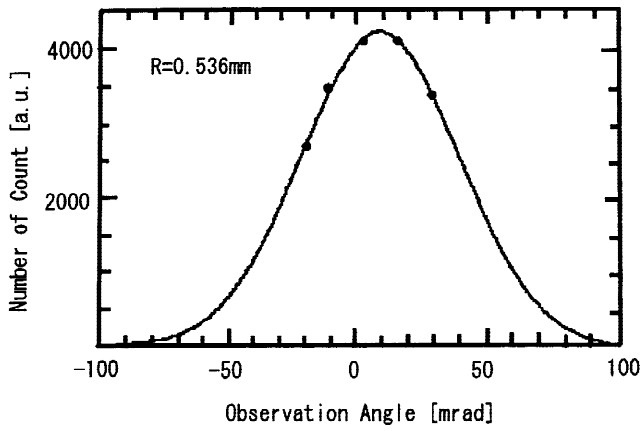

Fig. 15. Beam profile at a radial position.

function of the beam observation angle for respective radial position on the anode surface. One example is shown in Figure 15, from which we could estimate the divergence angle at the beam source. These processes were repeated for various radial positions on the anode surface, and the result is shown in Figure 16. This figure shows the beam divergence angle along the anode radius. In the same figure, the distribution of the maximum beam flux is shown also. We did not use any beam scattering foils in these experiments. The microdivergence angle of the proton beam on the anode surface was 20–60 mrad, which was significantly larger than the case with the nitrogen–oxygen beam shown above.

5. DISCUSSION

It is possible that the difference in microdivergence between the proton and nitrogen–oxygen beams may be partly due to any difference in enhancement in the two-specie bipolar space charge current density (i.e., the factor increase of the ion current density over the bipolar space charge current density). In the case of a nitrogen beam, the voltage, anode–cathode gap length, bipolar space charge current density, total peak ion current, and actual anode area were 350 kV, 6.5 mm, 13 A/cm^2, 300 A, and 41 cm^2. In the case of the proton beam, they were 200 kV, 6.5 mm, 21 A/cm^2, 700 A, and 41 cm^2. The enhancement factor was 0.56 in the case of the medium-mass beam, and 0.81 for the proton beam. The diode voltages in both cases were different, although the same diode was used in both cases. As these values were smaller than one in both cases, the source-limited ion extraction seemed to occur in our experiments shown here. The above calculation for the enhancement factor was not corrected for time-of-flight distance between the anode and detector. The beam transport between the anode and detector was strictly vacuum.

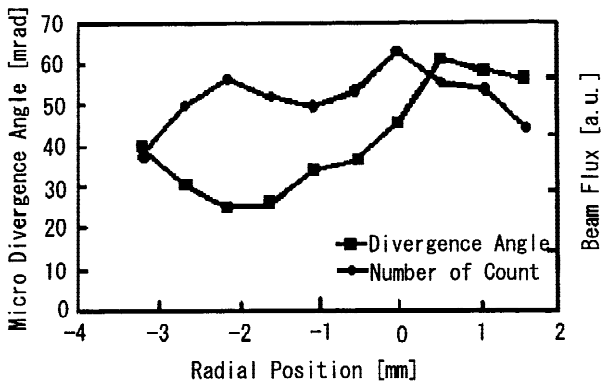

Fig. 16. Microdivergence angle and beam flux versus anode radial position.

Future plans include a scale-up of this diode to be fielded on the 800-kV RHEPP-1 facility at Sandia National Laboratories (SNL), in a collaboration between SNL and Tokyo Institute of Technology. Since RHEPP-1 is capable of reprating at up to 1 Hz, we may be able to study the suitability of rapidly operating a cryogenic diode. This has important future applications for producing rep-rated ICF and IFE drivers.

In the above experiments, we used CR-39 plastic solid state track detector (SSTD) for the particle counting. Although this plastic performs well in the severe noise conditions in our experiments, a more convenient particle detector is desired to get quick experimental results (Kasuya *et al.*, 1999). We thus plan to replace the CR-39 with a CCD camera in future experiments.

6. PROBABLE EXTENSION OF THE CRYOGENIC DIODE TO FUTURE RESEARH

After we developed a cryogenic diode to produce a very pure proton beam from hydrogen ice, one of the guiding principles in continuing our experiments has been the finding of a new research field under the combination of the pulsed power technology and the cryogenic engineering. Along this direction, we also proposed a new scientific field of the cryogenic targets ablated by pulsed ion beams (Kasuya & Okayama, 1999). Such kinds of preliminary experiments were also performed recently in collaboration between SNL and Tokyo Institute of Technology.

7. SUMMARY

Medium-mass ion beams of low microdivergence have been produced using a cryogenic anode source. The voltage, current, and current density values were 100–360 kV, 300 A, and 7.23 A/cm^2, respectively. The beam specie was mainly nitrogen with a small part (maybe one-third) of oxygen. Using a relatively simple and time-integrated technique, we obtained a divergence angle of 3–6 mrad at the ion source. A similar measurement for a proton beam (100–

https://doi.org/10.1017/S0263034601192207 Published online by Cambridge University Press

200 kV, 700 A, and 16.9 A/cm^2) with the same apparatus yielded 20–60 mrad. This suggests that further study is advisable of medium-mass ions as ICF and IFE drivers. Important subjects to be clarified during the study are species and charge-state spread, scaling upwards in ion current density, and other minor issues.

ACKNOWLEDGMENTS

This work was supported by the Ministry of Education, Sports, Science and Culture in Japan, together with the Japan Society for the Promotion of Sciences. The authors acknowledge also the support of Tokyo Institute of Technology (Yokohama and Tokyo, Japan), Sandia National Laboratories (Albuquerque, NM, USA) and Institute of Laser Engineering, Osaka University, Japan. We also acknowledge fruitful technical discussions with Drs. J. Quintenz, K. Matzen, C. Olson, T. Mehlhorn, R. Leeper, D. Hanson, M. Cuneo, B. Turman, D. Johnson, and T. Renk of Sandia National Laboratories, and Profs. S. Nakai, T. Yamanaka, H. Nishimura, and Y. Kozaki of Osaka University.

REFERENCES

Bluhm, H. (1992). Production and investigation of TW proton beams from an annular diode using strong radial magnetic insulation fields and a preformed anode plasma source. *Proc. IEEE* **80**, 995–1009.

Cuneo, M., Hanson, D. & Mehlhorn, T. (1999*a*). Generating high-brightness light ion beams for inertial fusion energy. *Proc. 17th IAEA Fusion Energy Conf.* **3**, 1123–1126.

Cuneo, M., Quintenz, J. & Olson, C. (1999*b*). Ion source requirements for light ion beam fusion. http://www.sandia.gov/pulspowr/hedicf/ionsource/.

Greenly, J., Hammer, D. & Kusse, B. (1988). Magnetically insulated ion diode with a gas-breakdown plasma anode. *J. Appl. Phys.* **63**, 1872–1876.

Hanson, D., Porter, J. & Williams, R. (1991). High-purity ion beam production at high current densities with a liquid-helium-cooled series-field-coil extraction ion diode. *J. Appl. Phys.* **70**, 2926–2938.

Kasuya, K. & Mitobe, K. (1987). Recent experimental results of cryogenic pulsed ion diodes. *Proc. 11th Int. Conf. Plasma Phys. and Control. Nucl. Fusion Res.* **3**, 161–166.

Kasuya, K., Ido, D., Okayama, H., Funatsu, M., Miyamoto, S., Nakai, S., Kawata, S., Okada, T. & Niu, K. (1999). Production, diagnostic and application of pulsed ion beams with light and medium mass; LIB (and MIB) program in Japan. *Fusion Eng. and Design* **44**, 319–326.

Kasuya, K. & Okayama, H. (1999). New method for thin-film formation with cryogenic diode and cryogenic target. *Fusion Eng. and Design* **44**, 327–330.

Mehlhorn, T. (1997). Intense ion beams for inertial confinement fusion. *IEEE Trans. Plasma Science* **25**, 1336–1356.

Olson, C. (1999). Final Rep. of Inertial Fusion Concepts Working Group. *APS Proc. Fusion Summer Studies*. New York: APS.

Quintenz, J., Bloomquist, D., Leeper, R., Mehlhorn, T., Olson, C., Olson, R., Peterson, R., Matzen, K. & Cook, D. (1996). Light ion driven inertial confinement fusion. *Prog. Nucl. Energy* **30**, 183–242.

APPENDIX: COMMENTS GIVEN BY REVIEWER

For HIF, the current mainline target requires a particle current of about 5 kA per beam, and each beam must hit a spot on the target that is elliptical with a minor axis of 0.18 cm. Typically, the beam radius at the final focus magnet is less than 10 cm, and the beam is ballistically focused over a distance of 5 m or more to the target. To hit a 2-mm radius spot at 5 m requires a beam divergence at a final focus of 0.4 mrad (or considerably less if the ion beam is not adequately charge neutralized). The present paper reports on a cryogenic ion source coupled with a high voltage diode. For a diode voltage of 400 kV, an ion current of 240 A is reported with a divergence of about 6 mrad. If the ions are all nitrogen ions with charge state $q = 1$, then $\beta \fallingdotseq 0.008$; and if these ions could be postaccelerated with no emittance growth to $\beta \geq 0.1$, then the divergence would be reduced to <0.6 mrad. In HIF accelerators, allowance for an emittance growth in the accelerator of a factor of 100 or more is typically included, so the typical HIF ion source should have an emittance of a factor of about 100 better than the emittance at the final focus. While the present paper has interesting results, it does not appear to be an adequate ion source for an HIF linear induction accelerator. If postacceleration with no emittance growth can be achieved, then the ion source of this paper may be of interest for a medium-mass ion IFE driver.